

Keysight Technologies

Thickness-dependent Electrical Properties
of Single-layer Graphene and Few-layer
Graphene: a Kelvin Force Microscopy Study

Application Note



Introduction

Graphene and its derivatives have emerged as a promising family of materials for nanoelectronics in a postsilicon era.¹ From an assembly point of view, these atomically thin carbon sheets of either single-layer graphene (SLG) or few-layer graphene (FLG) are well compatible with existing planar device architectures. On the other hand, one significant advantage of graphene-related nanomaterials is their highly tunable electrical properties such as carrier type or density, and rich electronic band structures. For instance, while single-layer graphene has a zero band gap, few-layer graphene differ from the intrinsic SLG in that they have various band gaps as a function of their number of layers. Consequently, a delicate control of graphene films with well-defined band gaps and thus to regulate their electronic properties is achievable.

Potential applications of graphene sheets as ultrathin transistors, sensors and other nanoelectronic devices require them supported on an insulating substrate. Therefore, a quantitative understanding of charge exchange at the interface and spatial distribution of the charge carriers is critical for the device design. While the impact of the substrate and interlayer interactions on the electronic structures of FLG is discussed extensively in prior theoretical simulation,^{2–7} experimental data of directly measuring the graphene-substrate interactions are lacking. In this note, we report that atomic force microscopy (AFM)-based technique Kelvin force microscopy (KFM) as an experimental means to investigate the local electrical properties of both single-layer and few-layer graphene films on silicon dioxide. The effect of the film thickness on the surface potential is detected and quantitative measurements are obtained.



Figure 1. An optical photograph of exfoliated graphene flakes with various thickness on a silicon dioxide substrate.

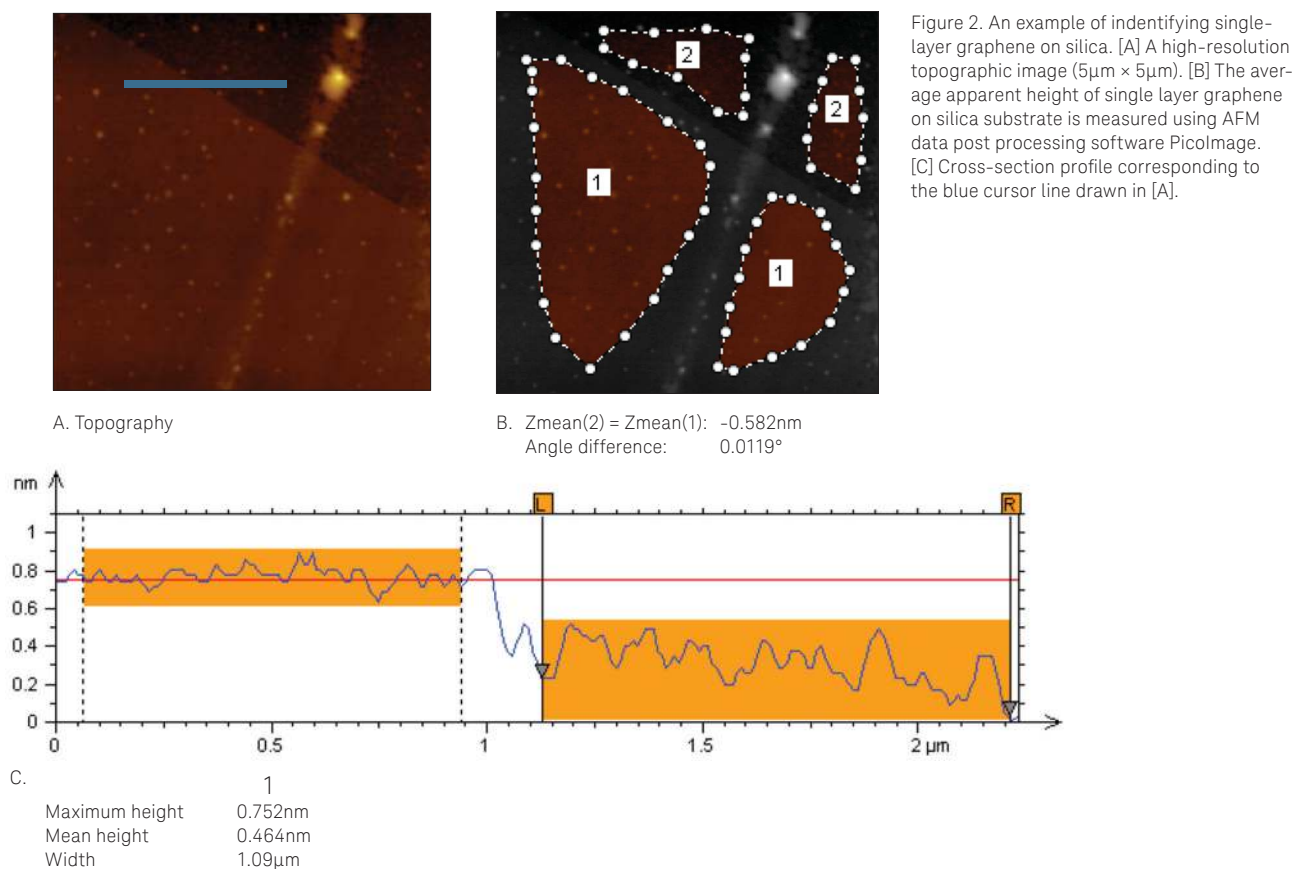
Single-pass Kelvin Force Microscopy

Traditional Kelvin force microscopy is implemented in a two-pass approach known as lift mode. In the lift mode, a first scan is taken to obtain the surface morphology, followed by positioning the tip at a certain distance above the sample. Quantitative mapping of a sample's surface potential is obtained in the second pass by guiding the tip along the surface contour and applying a second feedback control to null the tip/sample electrostatic interactions. The subsequent acquisition of topography and surface potential could lead to a mismatch between the two images due to the thermal drift effect. Furthermore, sensing the electrostatic forces at a remote tip-sample separation may have a negative impact on the detection sensitivity, thus affecting both the spatial resolution and the accuracy of surface potential measurements.

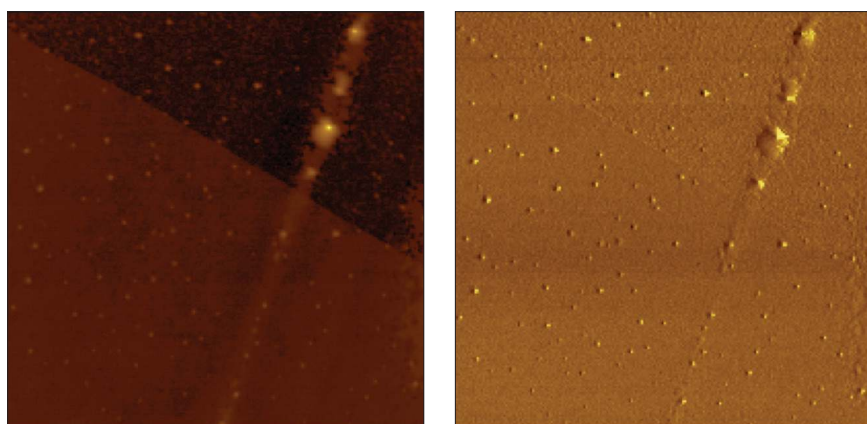
Multiple lock-in amplifiers have been introduced nowadays as an essential part of the electronics for scanning probe microscopes. For example, most of the Keysight Technologies, Inc. AFM platforms have the option to be incorporated with a MAC III or AAC III unit equipped with three dual phase lock-in amplifiers (LIAs) that allow the AC inputs to be converted into amplitude and phase signals. These digitally-controlled analog LIAs have a broad bandwidth up to 6 MHz to cover the operational bandwidth of the photodetector employed in the microscope. As a result, a single-pass KFM imaging is allowed by the simultaneous use of the probe flexural resonance frequency (ω_{mech} in the first LIA targeting the mechanical tip-sample interactions) for surface profiling and a much lower frequency (ω_{elec} in the second LIA for monitoring the electrostatic interactions) for sample surface potential measurements. In addition, the single-pass KFM at Keysight is operated in the intermittent regime, thus significantly enhancing the localized surface potential measurements.

Identify Single-layer Graphene on SiO₂ via High-resolution AFM Imaging

Up to date, the most widely used method to prepare graphene samples is mechanical exfoliation of graphite onto oxidized silicon surfaces. Figure 1 is an optical photograph of exfoliated graphene flakes on a silica substrate, in which various colors corresponding to different film thickness (or number of layers) are noticeably captured. A darker contrast is related to a thicker film. An example of identifying single layer graphene on silica by AFM imaging is shown in the high-resolution topographic image Figure 2A. The morphological



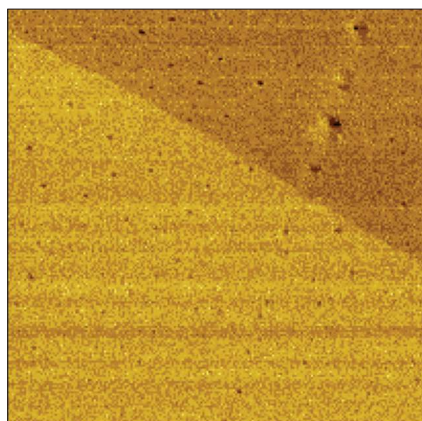
difference between the graphene film and the substrate is observed. The graphene layer is much smoother so individual granular features within the substrate area are resolved. Such conclusion is further supported by the cross-session cursor profile (Figure 2C, corresponding the blue line drawn in Figure 2A), in which a better view of the surface corrugation of graphene film vs. substrate is provided and quantified measurements of the surface roughness at each region can be derived. It shows that the typical peak-to-peak surface corrugation in the silica region is almost doubled compared to that of graphene layer. In addition, Figure 2C shows that the height of this graphene film is about 0.464 nm. Statistical measurement of the apparent height of a single graphene layer is performed using the “step height” function in AFM post processing software Picolmage (Figure 2B). The resulting value is 0.582 nm, similar to that derived from local cross-session measurement in Figure 2C. Although the interlayer spacing of HOPG is 0.34 nm in theory, practical AFM measurements of a single graphene layer on Si/SiO₂ always lead to higher values due to the weak sample/substrate interactions and presence of ambient species (nitrogen, oxygen, argon, or water) between SiO₂ and graphene and the graphene sheet and/or on the graphene sheet.⁸ Assuming the thickness of graphene films is governed by a linear relationship equation: $h = n \times t + t_0$, where n is an integer as the number of layers, t is the approximate theoretical thickness of each graphene layer, and t_0 is a systematic offset (i.e., independent of n), the best-fit values for t and t_0 based on a combined Raman scattering and AFM studies were 0.35 ± 0.01 nm and 0.33 ± 0.05 nm, respectively.⁹ Therefore, our experimentally measured apparent height of single-layer graphene on silica is in a good agreement with this model in the case of $n=1$.



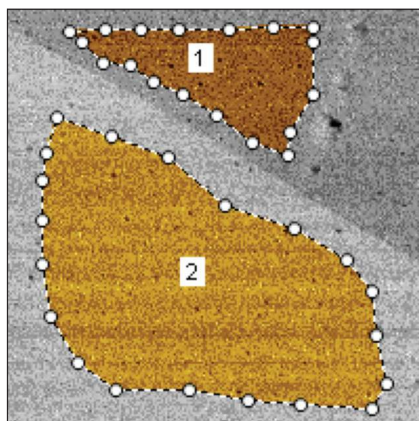
A. Topography

B. Phase

Figure 3. KFM imaging of single-layer graphene on silica. [A] A high-resolution topographic image ($6\mu\text{m} \times 6\mu\text{m}$). [B] and [C] Corresponding phase and surface potential images of [A], respectively. [D] Statistic measurements of the average variation in surface potential between single-layer graphene and silica substrate using AFM data post processing software PicoImage.



C. Surface Potential



D. $Z_{\text{mean}}(2) = Z_{\text{mean}}(1): 0.595\text{V}$
Angle difference: 22.6°

Differentiate and Quantify the Variation in Surface Potential Between Single-layer Graphene and a Silica Substrate

After locating a sample site containing single-layer graphene, *in situ* KFM imaging is conducted subsequently to measure the surface potential of the same area. Figure 3A is the topographic image that is almost identical to Figure 2A except that the scan size is slightly increased (from $5\mu\text{m} \times 5\mu\text{m}$ to $6\mu\text{m} \times 6\mu\text{m}$). Figure 3B and 3C are simultaneously acquired phase and surface potential images, respectively. Despite the solid fact that phase contrasts have been proven to be associated with materials mechanical nature (stiffness, friction) or adhesive properties and can be utilized to distinguish different components of heterogeneous polymer or other thin film materials, it turns out the sensitivity of phase imaging may not be sufficient in this extreme case dealing with only a monolayer of carbon atoms. Figure 3B is such homogenous that contrast variations between graphene layer and bare substrate is negligible. Therefore, it is very encouraging that different contrasts are observed in surface potential image Figure 3C and their boundary is matching exactly to that between the two regions (in the corresponding topographic image Figure 3A). At this point, it is demonstrated that KPFM technique can complement phase imaging and serve as an effective means to detect graphene-related nanomaterials on a silica substrate.

In addition, Figure 3C indicates that the surface potential of single-layer graphene is slightly higher than that of silica. Quantified measurement in Figure 3D shows the surface potential variation between two different materials is about 60mV.

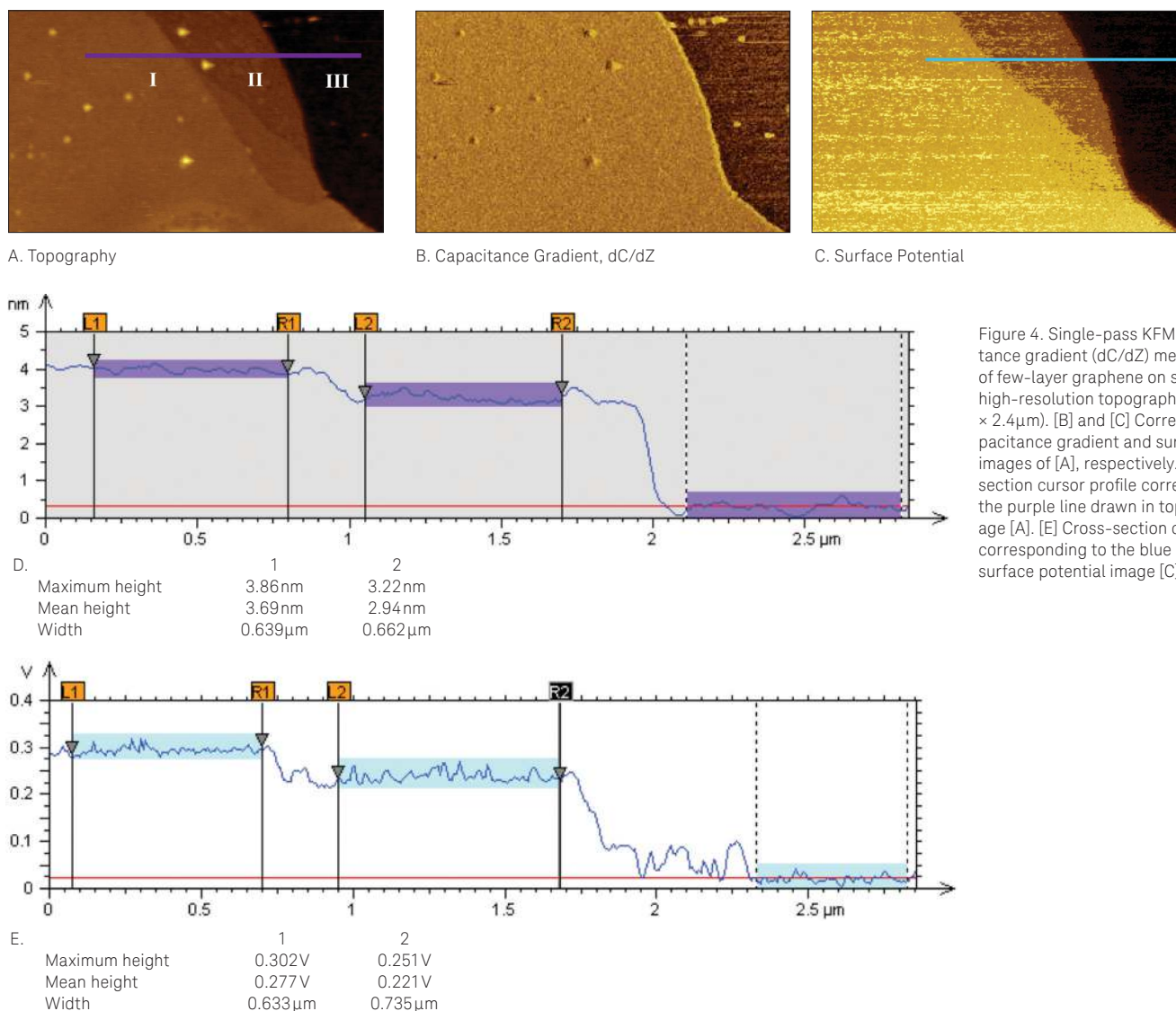


Figure 4. Single-pass KFM and capacitance gradient (dC/dZ) measurements of few-layer graphene on silica. [A] A high-resolution topographic image ($4\mu\text{m} \times 2.4\mu\text{m}$). [B] and [C] Corresponding capacitance gradient and surface potential images of [A], respectively. [D] Cross-section cursor profile corresponding to the purple line drawn in topographic image [A]. [E] Cross-section cursor profile corresponding to the blue line drawn in surface potential image [C].

Single-pass KFM and Capacitance Gradient (dC/dZ) Measurements of Few-layer Graphene

More valuable data comes from our single-pass Kelvin force microscopy and capacitance gradient (dC/dZ) measurements of few-layer graphene samples. A typical example is presented in Figure 4. Multiple steps are well resolved and three main regions (labeled as I, II, and III, respectively) are distinguished in topography image (Figure 4A). Figure 4D is the cross-section profile corresponding to the purple line drawn in Figure 4A, from which the region I is indicated to be about 0.75nm higher than region II using region III as a background baseline. This value is in good agreement with two times of the HOPG interlayer spacing (0.34nm). Actually, this calculated bilayer change in the film thickness is further confirmed by a well-defined single atomic step resolved between region I and region II in Figure 4A. Once again, the corresponding phase image (data not shown here) is similar to Figure 3B and thus hard to be used as an evidence to differentiate few-layer graphene films from a bare silica substrate. Furthermore, although surface potential measurements prove to be sufficient to distinguish single-layer graphene from SiO_2 , the

dependence of surface potentials on the film thickness (illustrated in Figure 4C) brings an unavoidable complexity to the case of few-layer graphene. Additional probing based on materials other electric properties will substantially benefit for a successful identification of region III as a substrate area. At this point, we are taking the advantage of the availability of a third LIA by connecting it directly to the photodetector and monitor the tip response at the frequency of $2\omega_{\text{elec}}$. The oscillation of the tip induced by the electrostatic force at this $2\omega_{\text{elec}}$ frequency is in proportional to the capacitance gradient (dC/dZ), which is related to the local dielectric permittivity of the sample. It is exciting to see that both region I and region II, regardless of containing different graphene layers, exhibit a homogenous contrast that is brighter than that of region III in dC/dZ image Figure 4B. Such results can be validated by the fact that the dielectric constant of graphite material ($\epsilon=10-15$) is much higher than that of silica ($\epsilon=3.9$). Therefore, it is demonstrated here that the combination of KFM and capacitance gradient (dC/dZ) measurements allow an unambiguous distinction between interface layer and multi-layer graphene.

A layer-dependent behavior is detected in our surface potential measurements of FLG films, evidenced by the observation that the thicker film in region I has a brighter contrast than that of region II in Figure 4C. The cross-sectional view of the blue line drawn in surface potential image indicate that the variation of surface potential between graphene film at region II (assigned to be nine layers based on an apparent height of 2.94 nm derived in Figure 2C) vs. silica substrate is about 221 mV, which is much higher than the value of 60 mV that is revealed in Figure 3D in the case of a single-layer graphene. Continued rise of two additional layers results into a further increase of 56 mV in region I with respect to region II.

The conclusion that FLG surface potential change monotonically with graphene layers based on our KFM studies is consistent to the observations by many other groups. For example, Filleter *et al* found a surface potential reduction of 135 mV for single layer as compared to bilayer graphene grown epitaxially on a SiC substrate.¹⁰ In contrast to a linear relationship between FLG thickness and the number of layers, the variation of surface potential between the two neighboring layers decrease exponentially when the thickness of graphene films goes up. It is reported that FLG surface potential may approach a “bulk” value for samples with five or more graphene samples.¹¹ To the best of our knowledge, the possible threshold has been extended to ten layers by Lee *et al* that a tiny surface potential difference between seven- and nine-layers of exfoliated graphene on silica has been resolved.¹² Here, we report our successful differentiation and quantitative measurement of the surface potential between nine- and eleven-layer graphene films.

Conclusions

Kelvin force microscopy is employed to investigate the local electric properties of either single-layer or few-layer graphene films on a silicon substrate. A thickness-dependent surface potential behavior of graphene films is observed and quantitative measurements of surface potentials for both single-layer graphene and few-layer graphene are reported. In addition, it proves that local electrical property-based measurements (surface potential or/and capacitance gradient) have a higher sensitivity than mechanical property-based phase imaging in both detection and differentiation of graphene sheets with either single-layer or multilayer structures.

Acknowledgements

The graphene samples that were used in studies described in this application note were kindly provided by Dr. Ryan Cooper and Prof. Jeffrey W. Kysar from Columbia University.

References

- Berger at al. Electronic confinement and coherence in patterned epitaxial graphene. *Science* 2006, 312, 1191–1196.
- Guinea at al. Charge distribution and screening in layered graphene systems. *Phys. Rev. B* 2007, 75, 235433.
- McCann at al. Asymmetry gap in the electronic band structure of bilayer graphene. *Phys. Rev. B* 2006, 74, 161403.
- Min at al. Ab initio theory of gate induced gaps in graphene bilayers. *Phys. Rev. B* 2007, 75, 155115.
- Zhou at al. Substrate-induced bandgap opening in epitaxial graphene. *Nat. Mater.* 2007, 6, 770–775.
- Adam at al. A self-consistent theory for graphene transport. *Proc. Natl. Acad. Sci.* 2007, 104, 18392.
- Katsnelson at al. Electron scattering on microscopic corrugations in graphene. *Phil. Trans. R. Soc. A* 2008, 366, 195.
- Ishigami at al. Atomic structure of graphene on SiO₂. *Nano Lett.* 2007, 6, 1643–1648.
- Gupta at al. Raman scattering from high-frequency phonons in supported n-graphene layer films. *Nano Lett.* 2006, 12, 2667–2673.
- Filletter at al. Local work function measurements of epitaxial graphene. *Appl. Phys. Lett.* 2008, 93, 133117.
- Datta at al. Surface potentials and layer charge distributions in few-layer graphene films. *Nano Lett.* 2009, 9, 7–11.
- Lee at al. The interlayer screening effect of graphene sheets investigated by Kelvin probe force microscopy. *Appl. Phys. Lett.* 2009, 95, 222107.

For more information on Keysight Technologies' products, applications or services, please contact your local Keysight office. The complete list is available at: www.keysight.com/find/contactus

Americas

Canada	(877) 894 4414
Brazil	55 11 3351 7010
Mexico	001 800 254 2440
United States	(800) 829 4444

Asia Pacific

Australia	1 800 629 485
China	800 810 0189
Hong Kong	800 938 693
India	1 800 112 929
Japan	0120 (421) 345
Korea	080 769 0800
Malaysia	1 800 888 848
Singapore	1 800 375 8100
Taiwan	0800 047 866
Other AP Countries	(65) 6375 8100

Europe & Middle East

Austria	0800 001122
Belgium	0800 58580
Finland	0800 523252
France	0805 980333
Germany	0800 6270999
Ireland	1800 832700
Israel	1 809 343051
Italy	800 599100
Luxembourg	+32 800 58580
Netherlands	0800 0233200
Russia	8800 5009286
Spain	0800 000154
Sweden	0200 882255
Switzerland	0800 805353
	Opt. 1 (DE)
	Opt. 2 (FR)
	Opt. 3 (IT)
United Kingdom	0800 0260637

For other unlisted countries:
www.keysight.com/find/contactus
 (BP-07-10-14)